

Task-Oriented Communications for Visual Navigation with Edge-Aerial Collaboration in Low Altitude Economy

Zhengru Fang^{*}, Zhenghao Liu[‡], Jingjing Wang[‡], Senkang Hu^{*}, Yu Guo^{*}, Yiqin Deng^{*}, Yuguang Fang^{*}

^{*}Hong Kong JC STEM Lab of Smart City and Department of Computer Science,
City University of Hong Kong, Hong Kong, [‡]Beihang University, China.

Email: {zhefang4-c, senkang.forest}@my.cityu.edu.hk,
{21371445, drwangjj}@buaa.edu.cn, {yu.guo, yiqideng, my.fang}@cityu.edu.hk

Abstract—To support the Low Altitude Economy (LAE), it is essential to achieve precise localization of unmanned aerial vehicles (UAVs) in urban areas where global positioning system (GPS) signals are unavailable. Vision-based methods offer a viable alternative but face severe bandwidth, memory and processing constraints on lightweight UAVs. Inspired by mammalian spatial cognition, we propose a task-oriented communication framework, where UAVs equipped with multi-camera systems extract compact multi-view features and offload localization tasks to edge servers. We introduce the Orthogonally-constrained Variational Information Bottleneck encoder (O-VIB), which incorporates automatic relevance determination (ARD) to prune non-informative features while enforcing orthogonality to minimize redundancy. This enables efficient and accurate localization with minimal transmission cost. Extensive evaluation on a dedicated LAE UAV dataset shows that O-VIB achieves high-precision localization under stringent bandwidth budgets. Code and dataset will be made publicly available at: github.com/fangzr/TOC-Edge-Aerial.

Index Terms—Visual navigation, information bottleneck, edge inference, task-oriented communications.

I. INTRODUCTION

The low altitude economy (LAE) envisions large-scale deployment of unmanned aerial vehicles (UAVs) for applications such as cargo delivery, traffic surveillance, and emergency response [1]–[4]. Achieving precise and resilient localization is foundational to these LAE applications. Although global navigation satellite systems (GNSS) are widely used, they remain vulnerable to jamming, spoofing, and multipath effects in urban canyons, rendering them unreliable in contested or GNSS-denied environments [5].

Conventional alternatives—including inertial navigation, magnetic sensing, or acoustic positioning—can partially mitigate these limitations, but face accuracy degradation due to sensor drift, calibration complexity, or environmental noise. While cryptographic GNSS authentication and time-of-arrival (ToA) signal processing offer security or precision benefits, they often demand expensive hardware upgrades and incur significant energy and latency costs, limiting their suitability for lightweight UAV platforms [6].

To address these constraints, vision-based approaches are gaining traction. Recent studies show that visual-inertial odometry with artificial markers can provide sub-meter accuracy under occlusions and urban interference [7]. Collaborative visual SLAM

techniques also enable multiple UAVs to jointly construct dense 3D maps [8]. These methods, while accurate, are often resource-intensive, making real-time onboard execution impractical for low-power UAVs.

The concurrent emergence of edge computing provides a promising path forward: rather than executing complex localization pipelines onboard, UAVs can extract salient visual features and delegate heavy computation to ground-based edge servers. In this paradigm, task-oriented communication (TOC) [9] ensures that only task-relevant, compressed features are transmitted—significantly reducing bandwidth consumption. Such strategies have been explored for cooperative learning and detection [10], [11] and further extended to covert or privacy-aware collaboration in aerial networks [12].

Motivated by these insights, we develop a novel UAV-edge collaboration system designed for robust visual localization in LAE settings. We introduce the Orthogonally-constrained Variational Information Bottleneck (O-VIB) encoder, which compresses high-dimensional, multi-view features extracted by UAV-mounted cameras. O-VIB integrates automatic relevance determination (ARD) to prune uninformative latent dimensions and enforces orthogonality among latent representations to reduce feature redundancy. This dual strategy ensures efficient encoding aligned with both task utility and transmission economy. Additionally, our work aligns with recent advances in multi-agent trajectory planning and federated computation offloading in air-ground networks [13]–[15], and complements new efforts in hierarchical intelligence for 6G LAE infrastructures [16].

Our contributions are summarized as follows:

- We propose O-VIB, a novel encoder incorporating orthogonality constraints and ARD-driven sparsification, that enables compact feature encoding that supports accurate localization at low communication cost.
- We introduce a large-scale, multi-camera UAV localization dataset, consisting of 357,690 frames with aligned RGB, depth, and semantic views, tailored to simulate realistic urban GNSS-denied scenarios.
- We validate O-VIB on a physical testbed and demonstrate its superiority in localization accuracy and bandwidth efficiency under LAE conditions.

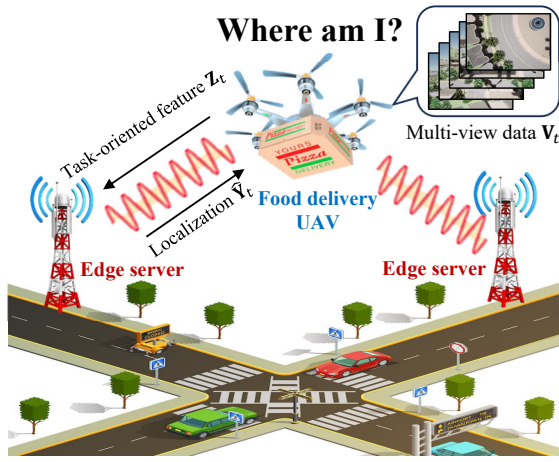


Fig. 1. The system model of Edge-aerial collaboration.

II. SYSTEM OVERVIEW

A. System Architecture and Problem Formulation

Consider a UAV-edge collaborative system operating in a GPS-denied urban environment, as illustrated in Fig. 1. We denote by \mathcal{U} the multi-camera UAV that captures multi-directional view $\mathcal{V} = \{v_1, v_2, \dots, v_M\}$ where $M = 5$ indicates our five-camera configuration (Front, Back, Left, Right, Down). The edge server, denoted by \mathcal{E} , maintains a geo-tagged feature database $\mathcal{D} = \{(f_i, l_i)\}_{i=1}^N$, where f_i represents the visual features and $l_i = (x_i, y_i, z_i)$ denotes the corresponding 3D position. The UAV captures multi-view images at time step t , represented as $\mathbf{V}_t = \{V_t^{(1)}, V_t^{(2)}, \dots, V_t^{(M)}\}$. For each view $m \in \{1, 2, \dots, M\}$, a feature extractor $\Phi(\cdot)$ generates high-dimensional features $\mathbf{X}_t^{(m)} = \Phi(V_t^{(m)}) \in \mathbb{R}^d$, where $d = 512$ in our implementation. The concatenated multi-view features are denoted as $\mathbf{X}_t = [\mathbf{X}_t^{(1)}, \mathbf{X}_t^{(2)}, \dots, \mathbf{X}_t^{(M)}] \in \mathbb{R}^{M \times d}$. Our objective is to accurately localize the UAV while minimizing communication overhead. Formally, we aim to solve:

$$\min_{\Theta} \mathbb{E}[\|\hat{\mathbf{Y}}_t - \mathbf{Y}_t\|_2^2], \quad \text{s.t. } C(\mathbf{Z}_t) \leq C_{\max}, \quad (1)$$

where $\hat{\mathbf{Y}}_t$ represents the estimated UAV position, \mathbf{Y}_t is the ground truth position, Θ denotes the trainable parameters of our framework, \mathbf{Z}_t is the compressed representation transmitted from UAV to edge servers, $C(\cdot)$ is the communication cost function, and C_{\max} is the maximum allowable communication bandwidth. The extracted features \mathbf{x} , the encoded features \mathbf{z} , and the position estimation \mathbf{y} are instantiated by random variables \mathbf{X}_t , \mathbf{Z}_t and \mathbf{Y}_t , respectively.

B. Wireless Communication Model

For the wireless link between the UAV and an edge server, we adopt the Shannon capacity model. Thus, the achievable data rate R (in bits/s) can be expressed as:

$$R = B \log_2 \left(1 + \frac{P \cdot g}{N_0 \cdot B} \right), \quad (2)$$

where B is the channel bandwidth, P is the transmit power, g is the channel gain incorporating path loss, shadowing, and fading effects, while N_0 is the noise power spectral density. The channel

gain g is modeled as $g = g_0 \cdot \left(\frac{d_0}{d}\right)^\alpha \cdot 10^{\frac{\xi}{10}} \cdot |h|^2$, where g_0 is the reference channel gain at distance d_0 , d is the distance between UAV and edge server, α is the path loss exponent (typically 2-4 in urban environments), $\xi \sim \mathcal{N}(0, \sigma^2)$ represents log-normal shadowing with standard deviation σ , and h accounts for small-scale fading. The transmission delay for sending compressed features \mathbf{Z}_t is given by $\tau = \frac{|\mathbf{Z}_t|}{R}$, where $|\mathbf{Z}_t|$ denotes the bit-size of the compressed representation.

C. Multi-View Visual Localization Pipeline

Our multi-view visual localization pipeline comprises three main components: Feature Extraction, Task-Oriented Feature Compression, and Edge-Based Position Inference.

In the **Feature Extraction** stage, each camera view is processed through a CLIP-based visual encoder $\Phi(\cdot)$ to extract discriminative features. For every view $m \in \{1, 2, \dots, M\}$ at time t , the encoded feature is computed as

$$\mathbf{X}_t^{(m)} = \Phi(V_t^{(m)}). \quad (3)$$

As shown in Fig. 2, during the **Task-Oriented Feature Compression** phase, the extracted multi-view features \mathbf{X}_t are compressed into a task-relevant representation \mathbf{Z}_t using a VIB-based encoder with orthogonality constraints, i.e.

$$\mathbf{Z}_t = \mathcal{E}(\mathbf{X}_t; \Theta_E), \quad (4)$$

where $\mathcal{E}(\cdot)$ denotes our proposed encoding function parameterized by Θ_E . As shown in Fig. 3, in the **Edge-Based Position Inference** stage, the compressed representation is transmitted to the edge server, which applies multi-view attention fusion to estimate the UAV's position

$$\hat{\mathbf{Y}}_t = \mathcal{F}(\mathbf{Z}_t; \Theta_F, \mathcal{D}). \quad (5)$$

In this equation, $\mathcal{F}(\cdot)$ represents the fusion and localization function with parameters Θ_F , and \mathcal{D} refers to a geo-tagged database used for querying position information. The position estimation integrates a hybrid method that combines direct regression and retrieval-based inference

$$\hat{\mathbf{Y}}_t = \eta \cdot \hat{\mathbf{Y}}_t^{reg} + (1 - \eta) \cdot \hat{\mathbf{Y}}_t^{ret}, \quad (6)$$

where $\hat{\mathbf{Y}}_t^{reg}$ is the regressed position, $\hat{\mathbf{Y}}_t^{ret}$ is the retrieved position from the database, and $\eta \in [0, 1]$ is an adaptive weight that balances the two estimates based on confidence scores. It is noted that the above end-to-end pipeline is designed to optimize the trade-off between localization accuracy and communication efficiency, thereby enabling precise UAV navigation in GPS-denied environments with constrained wireless bandwidth.

III. METHODOLOGY

A. Task-Oriented Feature Extraction

To enable discriminative localization under limited bandwidth, we employ a CLIP-based vision backbone for robust multi-view feature extraction. Each image $V_t^{(m)}$ is processed via a shared feature extractor $\Phi(\cdot)$ implemented using the CLIP Vision Transformer (ViT-B/32), pretrained on large-scale natural image-text pairs. The encoder $\Phi(\cdot)$ first applies a learned preprocessing

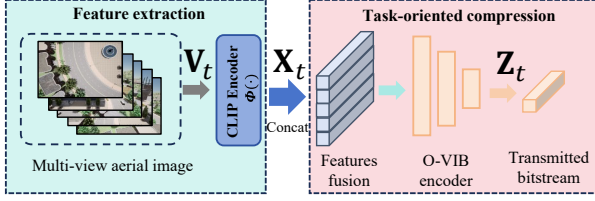


Fig. 2. Feature-extraction and task-oriented compression pipeline executed on board the UAV.

function $\psi(\cdot)$ that resizes, normalizes, and tokenizes the image into a sequence of visual patches. The feature encoding is obtained as:

$$\mathbf{X}_t^{(m)} = \Phi(V_t^{(m)}) = f_{\text{CLIP}}(\psi(V_t^{(m)}); \theta_\Phi) \in \mathbb{R}^d, \quad (7)$$

where $f_{\text{CLIP}}(\cdot)$ denotes the CLIP image encoder, parameterized by θ_Φ , while $d = 512$ is the dimensionality of the output embedding space for ViT-B/32. We normalize the extracted features to lie on the unit hypersphere to improve numerical stability and facilitate cosine similarity-based downstream retrieval, which yields $\tilde{\mathbf{X}}_t^{(m)} = \frac{\mathbf{X}_t^{(m)}}{\|\mathbf{X}_t^{(m)}\|_2}, \forall m \in \{1, \dots, M\}$. Besides, the final multi-view feature tensor is constructed by concatenating view-wise embeddings $\mathbf{X}_t = [\tilde{\mathbf{X}}_t^{(1)}; \tilde{\mathbf{X}}_t^{(2)}; \dots; \tilde{\mathbf{X}}_t^{(M)}] \in \mathbb{R}^{M \times d}$. This high-dimensional, view-aligned descriptor \mathbf{X}_t captures a rich, panoramic representation of the UAV's surroundings.

B. Task-Oriented Feature Compression

The high-dimensional multi-view descriptor $\mathbf{X}_t \in \mathbb{R}^{M \times d}$ provides comprehensive visual information about the UAV's surroundings. However, due to stringent communication constraints in UAV-edge collaborative systems, it is necessary to compress this descriptor into a compact task-relevant representation [17]. The IB principle provides an effective theoretical framework for addressing this challenge. Specifically, IB seeks an optimal stochastic encoder $q_\phi(\mathbf{z}|\mathbf{x})$ that generates a latent representation \mathbf{z} by achieving two conflicting goals: minimizing the mutual information $I(\mathbf{x}; \mathbf{z})$ to ensure compactness, while maximizing the mutual information $I(\mathbf{z}; \mathbf{y})$ to retain task-relevant information about the UAV's position \mathbf{y} . The IB optimization problem can thus be formulated as

$$\min_{\phi} \underbrace{\beta I(\mathbf{x}; \mathbf{z})}_{\text{Transmission}} - \underbrace{I(\mathbf{z}; \mathbf{y})}_{\text{Accuracy}}, \quad (8)$$

where the non-negative hyperparameter β controls the trade-off between feature compression (transmission efficiency) and localization accuracy.

1) *Why Automatic Relevance Determination (ARD)?*: The optimization problem in (8) already performs task-oriented rate-relevance trade-off, yet it counts every latent dimension equally. In practice, many coordinates are dispensable. We impose an *ARD sparsifier* by choosing for each z_i the *log-uniform* prior $p(z_i) \propto |z_i|^{-1}$ [18]. Its heavy tail is scale-invariant and assigns virtually no mass near zero, therefore encouraging uninformative coordinates to collapse automatically.

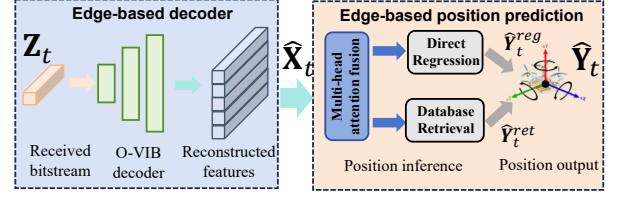


Fig. 3. Edge-side decoding and position-prediction pipeline running on RSU servers.

Let $\mathbf{x} \in \mathbb{R}^{M \times d}$ be the concatenated view features of one frame. The encoder is a diagonal Gaussian, which is formulated as

$$q_\phi(\mathbf{z} | \mathbf{x}) = \mathcal{N}(\boldsymbol{\mu}_\phi(\mathbf{x}), \text{diag } \boldsymbol{\sigma}_\phi^2(\mathbf{x})), \quad \mathbf{z} = \boldsymbol{\mu} + \boldsymbol{\sigma} \odot \boldsymbol{\epsilon}, \quad \boldsymbol{\epsilon} \sim \mathcal{N}(\mathbf{0}, \mathbf{I}).$$

The KL divergence between a univariate Gaussian posterior and the log-uniform prior admits an accurate analytic fit

$$\mathcal{D}_{\text{ARD}}(\boldsymbol{\mu}_\phi, \log \boldsymbol{\sigma}_\phi^2) = \frac{1}{B} \sum_{i=1}^k \left[k_1 \sigma(k_2 + k_3 \log \alpha_i) - \frac{1}{2} \log(1 + e^{-\log \alpha_i}) \right] \approx \text{KL}(q_\phi(\mathbf{z} | \mathbf{x}) \| p(\mathbf{z})), \quad (9)$$

where $\alpha_i := \sigma_i^2 / \mu_i^2$, and the predetermined coefficients are $(k_1, k_2, k_3) = (0.63576, 1.87320, 1.48695)$. B represents the minibatch size. According to **Theorem 1**, the traditional IB objective (8) is upper-bounded by the ARD-regularized variational objective in (13).

Lemma 1: Let $q_\phi(\mathbf{z} | \mathbf{x})$ be any encoder and let $p(\mathbf{z})$ be an arbitrary prior. Define the variational mutual information $I_{q_\phi}(\mathbf{x}; \mathbf{z}) := \text{KL}(q_\phi(\mathbf{x}, \mathbf{z}) \| q_\phi(\mathbf{x}) q_\phi(\mathbf{z}))$ and the marginal $q_\phi(\mathbf{z}) = \int q_\phi(\mathbf{z} | \mathbf{x}) p(\mathbf{x}) d\mathbf{x}$. Then

$$\begin{aligned} I_{q_\phi}(\mathbf{x}; \mathbf{z}) &= \mathbb{E}_{\mathbf{x}} \left[\text{KL}(q_\phi(\mathbf{z} | \mathbf{x}) \| p(\mathbf{z})) \right] - \text{KL}(q_\phi(\mathbf{z}) \| p(\mathbf{z})) \\ &\leq \mathbb{E}_{\mathbf{x}} \left[\text{KL}(q_\phi(\mathbf{z} | \mathbf{x}) \| p(\mathbf{z})) \right]. \end{aligned} \quad (10)$$

If $p(\mathbf{z})$ is chosen coordinate-wise log-uniform ($p(z_i) \propto |z_i|^{-1}$) and q_ϕ is diagonal Gaussian, the inner KL admits the accurate analytic fit $\mathcal{D}_{\text{ARD}}(\boldsymbol{\mu}_\phi(\mathbf{x}), \log \boldsymbol{\sigma}_\phi^2(\mathbf{x}))$ of [18], so that

$$I_{q_\phi}(\mathbf{x}; \mathbf{z}) \leq \mathbb{E}_{\mathbf{x}} [\mathcal{D}_{\text{ARD}}(\mathbf{x})]. \quad (11)$$

Proof: Eq. (10) follows from the classical chain rule for KL divergence; dropping the second (non-negative) term yields the inequality. $\mathcal{D}_{\text{ARD}}(\boldsymbol{\mu}_i, \log \sigma_i^2) \approx \text{KL}(q_\phi(\mathbf{z} | \mathbf{x}) \| p(\mathbf{z}))$, which Molchanov *et al.* show has a maximum absolute error below 10^{-3} for $\alpha_i \in [10^{-4}, 10^4]$ [18]. Replacing the conditional KL by its ARD fit gives Ineq. (11). ■

Lemma 2: For any decoder $p_\theta(\mathbf{y}|\mathbf{z})$ and joint distribution $p(\mathbf{z}, \mathbf{y})$, the mutual information between latent representation \mathbf{z} and task variable \mathbf{y} is lower-bounded by

$$I(\mathbf{z}; \mathbf{y}) \geq \mathbb{E}_{\mathbf{z}, \mathbf{y}} [\log p_\theta(\mathbf{y}|\mathbf{z})] - H(\mathbf{y}), \quad (12)$$

where $H(\mathbf{y}) = -\mathbb{E}_{\mathbf{y}} [\log p(\mathbf{y})]$ is the entropy of \mathbf{y} , a constant independent of model parameters (ϕ, θ) .

Proof: According to definition, we have $I(\mathbf{z}; \mathbf{y}) = H(\mathbf{y}) - H(\mathbf{y}|\mathbf{z})$. Since the KL divergence is always non-negative, we have $-H(\mathbf{y}|\mathbf{z}) \geq \mathbb{E}_{\mathbf{z}, \mathbf{y}} [\log p_\theta(\mathbf{y}|\mathbf{z})]$. Combining the above relations, we obtain $I(\mathbf{z}; \mathbf{y}) \geq \mathbb{E}_{\mathbf{z}, \mathbf{y}} [\log p_\theta(\mathbf{y}|\mathbf{z})] - H(\mathbf{y})$. ■

Theorem 1: *The traditional IB objective (8) is upper-bounded by the ARD-regularized variational objective*

$$\min_{\phi} \beta \mathbb{E}_{\mathbf{x}} [\mathcal{D}_{\text{ARD}}(\mathbf{x})] - \mathbb{E}_{\mathbf{z}, \mathbf{y}} [\log p_\theta(\mathbf{y} | \mathbf{z})], \quad (13)$$

which is tractable, differentiable, and automatically prunes uninformative latent coordinates by driving their contribution to near-zero.

Theorem 1 can be proven by combining **Lemmas 1** and **2**. Eq. (13) is what we optimize in practice. More explicitly, the first term is computed with (9), while the second term is tightened by a variational decoder $p_\theta(\mathbf{y} | \mathbf{z})$ as in **Lemma 2**.

2) *Orthogonality Under the IB Objective:* In our VIB-based encoder design, we compress the multi-view feature $\mathbf{x} \in \mathbb{R}^{M \times d}$ into a low-dimensional latent representation $\mathbf{z} \in \mathbb{R}^k$. Following the IB principle, we aim to minimize the mutual information $I(\mathbf{x}; \mathbf{z})$ (weighted by β) to limit bandwidth usage while ensuring \mathbf{z} retains sufficient information about \mathbf{x} for accurately predicting \mathbf{y} . To optimize the utilization of the limited information budget, we impose approximate row-orthogonality on the encoder's weight matrix \mathbf{W} . The proposition 1 shows that if $\mathbf{W}\mathbf{W}^\top$ is close to an identity matrix, the variance of each latent coordinate remains close to the average $\frac{1}{k} \text{Tr}(\mathbf{W}\Sigma_{\mathbf{x}}\mathbf{W}^\top)$. Consequently, no latent dimension collapses to near-zero variance, thereby avoiding redundancy in the latent representation.

Proposition 1: *Let $\mathbf{W} \in \mathbb{R}^{k \times d}$ denote the weight matrix of a Variational Information Bottleneck (VIB) encoder layer. Assume the approximate orthogonality condition*

$$\mathbf{W}\mathbf{W}^\top = \mathbf{I}_k + \Delta,$$

where \mathbf{I}_k denotes the $k \times k$ identity matrix and Δ is a symmetric perturbation matrix satisfying $\|\Delta\| \leq \varepsilon$ for a small $\varepsilon > 0$. Let $\mathbf{x} \in \mathbb{R}^d$ be an input vector with covariance $\Sigma_{\mathbf{x}} = \text{Cov}(\mathbf{x})$. Define the latent representation $\mathbf{z} = \mathbf{W}\mathbf{x}$, and let $a_i = \mathbf{w}_i \Sigma_{\mathbf{x}} \mathbf{w}_i^\top$ represent the variance along the i th latent dimension, where \mathbf{w}_i is the i th row of \mathbf{W} . Define the average variance $T = \frac{1}{k} \sum_{i=1}^k a_i = \frac{1}{k} \text{Tr}(\mathbf{W}\Sigma_{\mathbf{x}}\mathbf{W}^\top)$. Then, the minimum variance satisfies

$$\min_{1 \leq i \leq k} a_i \geq T - C\varepsilon,$$

where $C > 0$ is a constant dependent on $\|\Sigma_{\mathbf{x}}\|$.

Proof: We begin by observing the latent covariance $\Sigma_{\mathbf{z}} = \text{Cov}(\mathbf{z}) = \mathbf{W}\Sigma_{\mathbf{x}}\mathbf{W}^\top$. Hence, the total variance is given by

$$\text{Tr}(\Sigma_{\mathbf{z}}) = \sum_{i=1}^k \mathbf{w}_i \Sigma_{\mathbf{x}} \mathbf{w}_i^\top = \sum_{i=1}^k a_i,$$

and thus $T = \frac{1}{k} \text{Tr}(\Sigma_{\mathbf{z}})$. Under ideal orthogonality ($\mathbf{W}\mathbf{W}^\top = \mathbf{I}_k$), each dimension captures an equal variance T . However, approximate orthogonality in practice is modeled by decomposing \mathbf{W}

$$\mathbf{W} = \mathbf{W}_0 + \Delta\mathbf{W}, \quad \text{with} \quad \mathbf{W}_0\mathbf{W}_0^\top = \mathbf{I}_k,$$

and perturbation $\Delta\mathbf{W}$ satisfying $\mathbf{W}\mathbf{W}^\top = \mathbf{I}_k + \Delta$ and $\|\Delta\| \leq \varepsilon$. Considering $\mathbf{w}_i = \mathbf{w}_{0,i} + \Delta\mathbf{w}_i$, we obtain:

$$a_i = (\mathbf{w}_{0,i} + \Delta\mathbf{w}_i) \Sigma_{\mathbf{x}} (\mathbf{w}_{0,i} + \Delta\mathbf{w}_i)^\top.$$

Expanding this expression yields:

$$a_i = \underbrace{\mathbf{w}_{0,i} \Sigma_{\mathbf{x}} \mathbf{w}_{0,i}^\top}_{\text{Constant } T} + \underbrace{2\Delta\mathbf{w}_i \Sigma_{\mathbf{x}} \mathbf{w}_{0,i}^\top}_{\text{First-order term}} + \underbrace{\Delta\mathbf{w}_i \Sigma_{\mathbf{x}} \Delta\mathbf{w}_i^\top}_{\text{Second-order term}}.$$

Applying the Cauchy-Schwarz inequality and noting $\|\mathbf{w}_{0,i}\|_2 = 1$, the perturbation terms satisfy:

$$|2\Delta\mathbf{w}_i \Sigma_{\mathbf{x}} \mathbf{w}_{0,i}^\top| \leq 2\|\Delta\mathbf{w}_i\| \|\Sigma_{\mathbf{x}}\|,$$

and similarly, we have $|\Delta\mathbf{w}_i \Sigma_{\mathbf{x}} \Delta\mathbf{w}_i^\top| \leq \|\Delta\mathbf{w}_i\|^2 \|\Sigma_{\mathbf{x}}\|$. Since $\|\Delta\mathbf{w}_i\| \leq \varepsilon$, it follows that $|a_i - T| \leq 2\varepsilon \|\Sigma_{\mathbf{x}}\| + \varepsilon^2 \|\Sigma_{\mathbf{x}}\|$. For sufficiently small ε , we consolidate terms and define a constant C depending on $\|\Sigma_{\mathbf{x}}\|$, yielding $|a_i - T| \leq C\varepsilon$, and consequently we can prove $\min_{1 \leq i \leq k} a_i \geq T - C\varepsilon$. ■

According to **Proposition 1**, the approximate orthogonality of the encoder weights ensures that each latent dimension retains significant variance, avoiding collapsed dimensions. Under tight information bottleneck constraints, this property ensures each latent dimension effectively contributes to preserving relevant information, optimizing the latent representation \mathbf{z} with respect to the target variable \mathbf{y} . This behavior maximizes the mutual information $I(\mathbf{z}; \mathbf{y})$ subject to channel capacity constraints, enhancing the efficiency and accuracy of task-oriented data compression.

3) *Joint Encoding for Reducing Multi-View Redundancy:* Rather than compressing each camera stream in isolation, we concatenate the M view-wise embeddings into a single vector and pass it through one VIB-ARD encoder. This strategy exploits inter-view correlations so that the latent code stores only complementary information.

4) *Overall Training Objective:* Combining reconstruction fidelity, localization accuracy, ARD-based rate control, and orthogonality regularisation yields the composite loss

$$\begin{aligned} \mathcal{L}(\phi) = & \underbrace{\mathbb{E}[\|\mathbf{x} - \hat{\mathbf{x}}\|^2]}_{\text{Reconstruction}} + \underbrace{\alpha \mathbb{E}[\|\mathbf{y} - \hat{\mathbf{y}}\|^2]}_{\text{Localisation}} \\ & + \underbrace{\beta \mathbb{E}_{\mathbf{x}}[\mathcal{D}_{\text{ARD}}(\mathbf{x})]}_{\text{Information bottleneck}} + \underbrace{\gamma \|\mathbf{W}\mathbf{W}^\top - \mathbf{I}\|_F^2}_{\text{Orthogonality}}, \end{aligned} \quad (14)$$

where \mathbf{x} and $\hat{\mathbf{x}}$ are respectively the input and reconstructed multi-view features, \mathbf{y} and $\hat{\mathbf{y}}$ are respectively the ground-truth and predicted UAV positions. Furthermore, \mathcal{D}_{ARD} is the closed-form KL term in (9) that promotes sparsity of the latent code, while \mathbf{W} denotes the weight matrix of the encoder projection. The coefficients $\alpha, \beta, \gamma > 0$ balance the four competing objectives. Orthogonality guarantees that every retained latent dimension remains informative, whereas the ARD penalty drives superfluous coordinates toward zero variance, thereby enabling hard pruning after training.

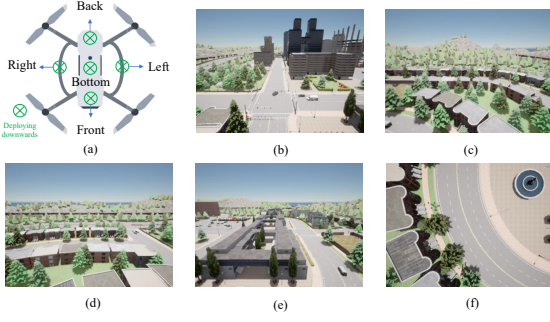


Fig. 4. Multi-camera UAV perception system and corresponding visual observations.

IV. PERFORMANCE EVALUATION

As shown in Fig. 4, we have collected a new dataset for visual navigation of UAVs in the CARLA simulator that mimics GNSS-denied flight over eight representative maps in cities¹. A UAV flies at a constant height following waypoints aligned with the road, changing direction randomly. Five onboard cameras capture images from different angles and directions, recording RGB, semantic, and depth images at a 400×300 pixels. A total of 357,690 multi-view frames are recorded, each labeled with the precise localization and rotation. As shown in Fig. 5, the framework is deployed on real hardware devices to evaluate the computation and communication latency of our proposed methods. Each UAV carries a Jetson Orin NX 8GB that encodes five camera streams and transmits compressed features to the nearby roadside units (RSUs) through wireless channels (IEEE 802.11). Two classes of RSU are deployed: (i) *Relay RSU*: Raspberry Pi 5 16 GB that forwards data by Gigabit Ethernet to a cloud edge server when overloaded; (ii) *Edge RSU*: Jetson Orin NX Super 16 GB that performs on-board inference.

Our primary metric is localization error (Euclidean distance to ground-truth pose). We additionally report the entropy–performance trade-off, i.e. how latent entropy after pruning correlates with accuracy, and measure end-to-end latency (UAV capture \rightarrow position estimation in edge server). Moreover, we compare our orthogonal VIB encoder to five advanced codecs: vanilla VIB [19], JPEG [20], H.264 [21], H.265/HEVC [22], and WebP [23]. All baselines are tuned to match our bitrate range for fair comparison.

Fig. 6 shows localization accuracy as the UAV–RSU link budget (in KB/s) is varied. Each scheme’s parameter set (e.g. latent dimension for VIB; quality factor for JPEG/H.264/H.265/WebP) is swept to identify Pareto-optimal points—minimizing error per KB/s. Features are encoded onboard, sent over IEEE 802.11, decoded at the RSU, and matched to a geo-tagged database; the nearest neighbor index yields the pose estimate. When network throughput is above 50 KB/s, all methods converge to a mean error of 10 m. When the bottleneck falls below 10 KB/s, O-VIB degrades most gracefully: at 8 KB/s it still achieves less than 10 m error, representing a 42.1% reduction versus vanilla VIB and a 62.6% reduction versus WebP. Embedding orthogonality

¹The code, demos and dataset will be made publicly available at: github.com/fangzi/TOC-Edge-Aerial

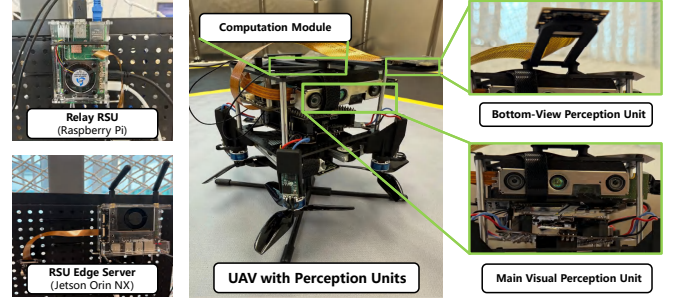


Fig. 5. Edge-enhanced UAV platform with integrated multiview perception and computing modules.

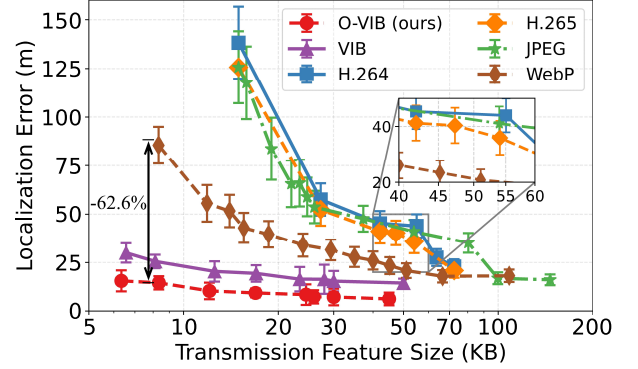


Fig. 6. Transmission feature size vs localization error.

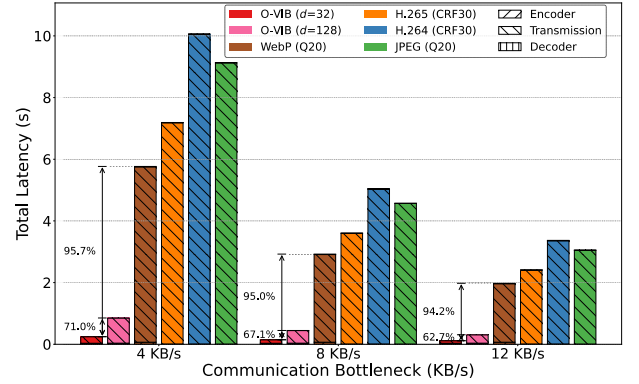


Fig. 7. Communication bottleneck vs latency.

thus prunes redundant latent dimensions while preserving task-critical information, making O-VIB far more robust under severe bandwidth constraints.

Fig. 7 shows end-to-end latency (encoding, transmission, decoding) under 4, 8, and 12 KB/s bottlenecks (poor channel conditions). At 4 KB/s, O-VIB achieves 0.24 s ($d = 32$) and 0.85 s ($d = 128$), while WebP, H.265, H.264, and JPEG incur 5.7 s, 7.1 s, 10.9 s, and 9.1 s. Compared to WebP, O-VIB reduces latency by 95.7%. At 8 KB/s, O-VIB drops to 0.15 s ($d = 32$) and 0.44 s ($d = 128$), while WebP remains at 2.9 s, achieving a 95.0% reduction. At 12 KB/s, O-VIB further lowers latency to 114.0 ms and 0.31 s, compared to WebP’s 1.9 s, realizing

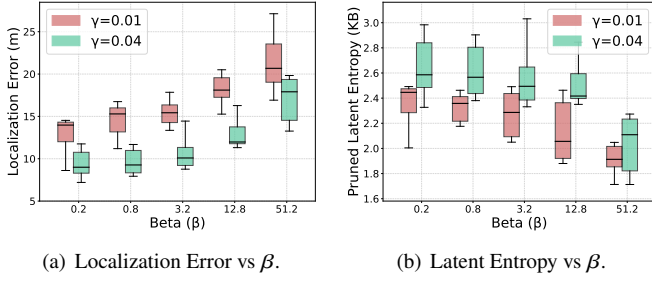


Fig. 8. Localization error and latent entropy vs β .

a 94.2% reduction. These results confirm that O-VIB maintains sub-second latency and achieves over an order of magnitude improvement under stringent bottlenecks.

Fig. 8 explores how the information-bottleneck weight β shapes the trade-off between compression and localization under two orthogonality strengths ($\gamma = 0.01, 0.04$). In Fig. 8(a), increasing β steadily reduces pruned latent entropy, confirming that the ARD term drives superfluous dimensions toward zero variance. At the same time, localization error rises from about 12 m to over 20 m for $\gamma = 0.01$ and from 9 m to 19 m for $\gamma = 0.04$, demonstrating the expected accuracy penalty of tighter compression. The $\gamma = 0.04$ curves consistently lie below $\gamma = 0.01$ in Fig. 8(a) while exhibiting higher entropy in Fig. 8(b), validating that stronger orthogonality preserves task-critical information and yields better localization at equivalent rates.

V. CONCLUSION

In this paper, we have proposed a task-oriented communication framework for visual navigation with Edge–Aerial collaboration for low altitude economy. Our contributions are twofold. First, we have developed a multi-camera Variational Information Bottleneck encoder augmented with an orthogonality constraint, which extracts ultra-compact, task-relevant features from five onboard RGB, semantic and depth views. Second, we have deployed and evaluated the complete system on both a new CARLA-derived dataset and a physical Jetson Orin NX/Raspberry Pi testbed, quantifying localization accuracy, latent-entropy trade-offs, and end-to-end latency. Extensive experiments have demonstrated that O-VIB maintains sub-10 m localization error at throughputs below 10 KB/s—reducing error by 42.1 % versus vanilla VIB and 62.6 % versus WebP—and achieves over three orders-of-magnitude lower latency than JPEG, H.264 and H.265. These results have confirmed that embedding orthogonality in an information-bottleneck framework yields highly informative, ultra-compact features that are robust under severe bandwidth constraints. We will release our dataset and code to accelerate future research in task-oriented aerial communications.

VI. ACKNOWLEDGEMENT

This work of Y. Fang was supported in part by the Hong Kong SAR Government under the Global STEM Professorship and Research Talent Hub, the Hong Kong Jockey Club under the Hong Kong JC STEM Lab of Smart City (Ref.: 2023-0108). This work of J. Wang was partly supported by the National Natural Science Foundation of China under Grant No. 62222101

and No. U24A20213, partly supported by the Beijing Natural Science Foundation under Grant No. L232043 and No. L222039, partly supported by the Natural Science Foundation of Zhejiang Province under Grant No. LMS25F010007. The work of S. Hu was supported in part by the Hong Kong Innovation and Technology Commission under InnoHK Project CIMDA. The work of Y. Deng was supported in part by the National Natural Science Foundation of China under Grant No. 62301300.

REFERENCES

- [1] Y. Deng, H. Zhang, X. Chen, and Y. Fang, “UAV-assisted MEC with an expandable computing resource pool: Rethinking the uav deployment,” *IEEE Wireless Communications*, vol. 31, no. 5, pp. 110–116, May 2024.
- [2] J. Wang, J. Wang, Z. Tong, Z. Jiao, M. Zhang, and C. Jiang, “ACBFT: Adaptive chained byzantine fault-tolerant consensus protocol for UAV Ad Hoc networks,” *IEEE Transactions on Vehicular Technology*, (DOI: 10.1109/TVT.2025.3548281), Mar. 2025.
- [3] J. Chen, J. Wang, J. Wang, and L. Bai, “Joint fairness and efficiency optimization for CSMA/CA-based multi-user MIMO UAV Ad Hoc networks,” *IEEE Journal of Selected Topics in Signal Processing*, vol. 18, no. 7, pp. 1311–1323, Oct. 2024.
- [4] J. Wang, L. Bai, J. Chen, and J. Wang, “Starling flocks-inspired resource allocation for ISAC-aided green Ad Hoc networks,” *IEEE Transactions on Green Communications and Networking*, vol. 7, no. 1, pp. 444–454, Mar. 2023.
- [5] H. Sathaye, M. Strohmeier, V. Lenders, and A. Ranganathan, “An experimental study of GPS spoofing and takeover attacks on UAVs,” in *USENIX security symposium (USENIX security)*, BOSTON, MA, Aug. 2022, pp. 3503–3520.
- [6] J. Wang, H. Du, Y. Liu, G. Sun, D. Niyato, S. Mao, D. I. Kim, and X. Shen, “Generative ai based secure wireless sensing for isac networks,” *arXiv preprint arXiv:2408.11398*, 2024.
- [7] F. Wang, Y. Zou, C. Zhang, J. Buzzatto, M. Liarokapis, E. del Rey Castillo, and J. B. P. Lim, “UAV navigation in large-scale GPS-denied bridge environments using fiducial marker-corrected stereo visual-inertial localisation,” *Automation in Construction*, vol. 156, p. 105139, Dec. 2023.
- [8] T. Zhang, L. Zhang, Y. Chen, and Y. Zhou, “CVIDS: A collaborative localization and dense mapping framework for multi-agent based visual-inertial SLAM,” *IEEE Transactions on Image Processing*, vol. 31, pp. 6562–6576, Oct. 2022.
- [9] X. Kang, B. Song, J. Guo, Z. Qin, and F. R. Yu, “Task-oriented image transmission for scene classification in unmanned aerial systems,” *IEEE Transactions on Communications*, vol. 70, no. 8, pp. 5181–5192, Aug. 2022.
- [10] Z. Fang, S. Hu, H. An, Y. Zhang, J. Wang, H. Cao, X. Chen, and Y. Fang, “PACP: Priority-aware collaborative perception for connected and autonomous vehicles,” *IEEE Transactions on Mobile Computing*, vol. 23, no. 12, pp. 15 003–15 018, 2024.
- [11] Z. Yuan, S. Rawlekar, S. Garg, E. Erkip, and Y. Wang, “Split computing with scalable feature compression for visual analytics on the edge,” *IEEE Transactions on Multimedia*, vol. 26, pp. 10 121–10 133, May 2024.
- [12] X. Hou, J. Wang, C. Jiang, X. Zhang, Y. Ren, and M. Debbah, “Uav-enabled covert federated learning,” *IEEE Transactions on Wireless Communications*, vol. 22, no. 10, pp. 6793–6809, Oct. 2023.
- [13] J. Huang, B. Wu, Q. Duan, L. Dong, and S. Yu, “A fast uav trajectory planning framework in ris-assisted communication systems with accelerated learning via multithreading and federating,” *IEEE Transactions on Mobile Computing*, (DOI: 10.1109/TMC.2025.3544903), pp. 1–16, 2025.
- [14] Z. Wang, J. Du, C. Jiang, Y. Ren, and X.-P. Zhang, “UAV-assisted target tracking and computation offloading in USV-based MEC networks,” *IEEE Transactions on Mobile Computing*, vol. 23, no. 12, pp. 11 389–11 405, Dec. 2024.
- [15] Z. Lin, Z. Chen, Z. Fang, X. Chen, X. Wang, and Y. Gao, “FedSN: A federated learning framework over heterogeneous LEO satellite networks,” *IEEE Transactions on Mobile Computing*, vol. 24, no. 3, pp. 1293–1307, 2025.
- [16] Q. Chen, Z. Wang, X. Chen, J. Wen, D. Zhou, S. Ji, M. Sheng, and K. Huang, “Space-ground fluid AI for 6G edge intelligence,” *arXiv preprint arXiv:2411.15845*, 2024.

- [17] Z. Fang, S. Hu, J. Wang, Y. Deng, X. Chen, and Y. Fang, "Prioritized information bottleneck theoretic framework with distributed online learning for edge video analytics," *IEEE Transactions on Networking*, DOI: 10.1109/TON.2025.3526148, Jan. 2025.
- [18] D. Molchanov, A. Ashukha, and D. Vetrov, "Variational dropout sparsifies deep neural networks," in *Proceedings of the 34th International Conference on Machine Learning (ICML)*, Sydney, Australia, July, 2017, pp. 2498–2507.
- [19] A. Furutanpey, P. Raith, and S. Dustdar, "Frankensplit: Efficient neural feature compression with shallow variational bottleneck injection for mobile edge computing," *IEEE Transactions on Mobile Computing*, vol. 23, no. 12, pp. 10 770–10 786, 2024.
- [20] G. K. Wallace, "The JPEG still picture compression standard," *IEEE Transactions on Consumer Electronics*, vol. 38, no. 1, pp. xviii–xxxiv, Feb. 1992.
- [21] ITU-T Recommendation H.264 and ISO/IEC 14496-10, *Advanced Video Coding for Generic Audiovisual Services*, International Telecommunication Union Std., 2003. [Online]. Available: <https://www.itu.int/rec/T-REC-H.264>
- [22] F. Bossen, B. Bross, K. Suhring, and D. Flynn, "HEVC complexity and implementation analysis," *IEEE Transactions on Circuits and Systems for Video Technology*, vol. 22, no. 12, pp. 1685–1696, Oct. 2012.
- [23] B. Li, J. Shi, W. Li, and H. Li, "WebP-JPEG transcoding detection by spotting re-compression artifacts with CNN-ViT for processing dual-domain features," *IEEE Transactions on Circuits and Systems for Video Technology*, vol. 34, no. 12, pp. 12 535–12 549, Dec. 2024.